Postprint of: Giosuè C., Pierpaoli M., di Perna C., Citterio B., Mangiaterra G., Ruello M. L., Tittarelli F., Properties of an innovative multi-functional finish for the improvement of indoor air quality, BUILDING AND ENVIRONMENT (2023), 110091, DOI: 10.1016/j.buildenv.2023.110091


# Properties of an Innovative Multi-functional Finish for the Improvement of Indoor Air Quality

Chiara Giosuè[a*], Mattia Pierpaoli[b], Costanzo di Perna[c], Barbara Citterio[d], Gianmarco Mangiaterra[d], Maria Letizia Ruello[a], Francesca Tittarelli[a,e]

[a] Department of Materials, Environmental Sciences and Urban Planning (SIMAU), Università Politecnica delle Marche, INSTM Research Unit, Ancona, 60131, Italy

[b] Department of Metrology and Optoelectronics, Faculty of Electronics, Telecommunication and Informatics, Gdańsk University of Technology, Gdańsk, 80-233, Poland

[c] Department of Industrial Engineering and Mathematical Sciences (DIISM), Università Politecnica delle Marche, via Brecce Bianche 12, Ancona, 60121, Italy

[d] Department of Biomolecular Science, University of Urbino 'Carlo Bo', Urbino, 61032, Italy

[e] ISAC-CNR, via Piero Gobetti 101, 40129 Bologna, Italy

* Correspondence to c.giosue@staff.univpm.it

## Abstract

Due to lifestyle changes, people spend most of their time indoors at present; thus, Indoor Air Quality (IAQ) is a matter of utmost importance. Multi-functional and innovative finishes can help to passively improve the IAQ, benefitting the health and comfort of occupants. For this study, reference and pre-mixed commercial mortars are compared to a new multi-functional hydraulic lime mortar for indoor finishes, in which conventional aggregates are substituted by a highly porous adsorbent material and biomass waste ashes. The up to 20% higher accessible porosity of the multi-functional finish led to lower density (30%), higher thermal insulation properties (30%), higher water vapor permeability (more than 40%), and improved moisture buffering capacity (three times higher), when compared to the reference mortar. Different types of photocatalytic agents ($TiO_2$) were also added into the new multi-functional hydraulic lime mortar, in order to investigate their effect on the de-polluting properties of the finish. Even if the photocatalytic efficiency remained unexpressed under indoor conditions, due to the predominance of the adsorption process, the de-polluting properties of the new mix were more than 30% higher than that of the reference mortar. The obtained results confirm that the developed innovative multi-functional finish—besides fulfilling the ordinary requirements—is

better than commercial mortars, as it can improve the IAQ passively, thus benefitting the health and comfort of occupants.

**Keywords**

*Indoor Air Quality (IAQ),) thermo-hygrometric behaviour, mould susceptibility, photocatalytic oxidation (PCO), adsorption, de-polluting properties.*

## 1. Introduction

The sustainability of the building sector has recently received increased attention, as around 40% of global carbon dioxide ($CO_2$) emissions are directly related to activities associated with the construction industry [1]. Consequently, several strategies have already been formulated to tackle their impact on the environment [2]. European Directives and laws have become stricter, in terms of energy efficiency; in particular, with more sealed buildings, if an appropriate air change rate is not guaranteed, the Indoor Air Quality (IAQ) may worsen as a result.

IAQ impacts the health, comfort, well-being, and cognitive performance of a building's occupants. As up to 90% of the population's time is spent indoors, on average [3], the risks related to being exposed to the different pollutants, such as Volatile Organic Compounds (VOCs), moulds, airborne particles, and inadequate levels of Relative Humidity (RH) are growing. Indoor humidity affects warm respiratory comfort, skin humidity, perceived IAQ, and well-being of occupants [4][5]. Moreover, high RH affects the durability of building materials and promotes biological attack of the surfaces, thus increasing maintenance costs [6]. Fungi and micro-organisms are also unhealthy for occupants, as they produce spores, allergens, toxins, and other metabolites that contribute to the degradation of IAQ [7] with consequent allergies, irritations, and respiratory and skin diseases. These negative effects can be short- or long-term, such as the well-known Sick Building Syndrome (SBS). SBS has been recognized by the U.S. National Institute for Occupational Safety and Health (NIOSH), the major cause of which is poor ventilation quality.

To settle this problem, the main techniques used at present to improve IAQ are ventilation, source control, and air cleaning [8] by means of active systems. However, thanks to their wide surface of exposure, building materials such as finishes can positively interact in a passive way with the surrounding environment [9], so these materials can help active systems to be more effective, using a lower amount of energy [10]. It has been demonstrated that highly porous materials applied indoors can act as buffers for RH which affects the indoor concentrations of humidity and VOC such toluene, as reported in XX, both numerically and by means of laboratory studies [11] [12].

Adsorption is one of the most effective de-polluting processes, in which a gas or liquid is passively removed from a fluid and transferred on the solid surface of the adsorbent, where the adsorbate covers the surface of the adsorbent with a molecular layer. The capturing methods differ in terms of the polarity (electrostatic forces), molecular weight (the higher the molecular weight, the higher the boiling temperature and the easier the deposition on the absorbent surface), and size (molecular sieves) of the adsorbate and adsorbent. As it is focused on the surface of the solid, the adsorption process requires a high specific surface of the solid adsorbent and a high solid–fluid contact area. Therefore, in order to obtain high removable efficiency of pollutants, very porous materials with a wide specific surface area (of about 300–3000 $m^2/g$) are required as adsorbents.

Heterogeneous Photocatalytic Oxidation (PCO) also represents a promising option to ensure healthier environments, exploring the possibilities of the use of nanotechnology in building materials [13][14]. PCO is a superficial phenomenon [15], induced when a photocatalytic agent, such as titanium dioxide ($TiO_2$), is added to a finish—either in bulk or as coating—for the mineralization of adsorbed pollutants into less harmful compounds. This process involves different steps [16][17]: PCO first requires UVA light wavelengths (320–400 nm) to activate the agent, generating a hole/pair. Then, the pollutants are adsorbed onto the $TiO_2$. PCO capacity is significantly affected by the presence of macro/micro pores [18][19] and hydraulic lime mortars generally have higher de-polluting properties than cement-based ones [16][20][19][21][22], due to the higher presence of micro-porosity; on the other hand, the higher quantity of gel pores (nanopores) than in cementitious products may hide the catalytic sites [18][19][23].

To improve the sustainability of finishes [24] [25], biomass by-products (e.g., ashes from the thermal valorisation of biomasses) have been used as unconventional aggregates [26]. Biomass ashes are considered carbon neutral as, in binder-based materials, they bind the same amount of $CO_2$ released in the combustion process [27]. Ashes typically contain silicon, calcium, potassium, phosphorus, manganese, iron, zinc, sodium, and boron, in the form of oxides, and studies have demonstrated that their use does not negatively influence the ecotoxicity of mortars [28]. Rather, they generally improve the mechanical and durability properties of the resulting concrete/mortar products, while also lowering the release of hazardous elements [29]. “Green” building materials containing biomass ashes able to decrease level of ozone [30] and indoor Volatile Organic Compound (VOC) de-pollution properties due to their adsorption ability [31], have already been successfully developed [31]. Biomass ashes also enhance the thermo-hygrometric performance of finishes/renders [32] [33][34]. As long as an RH level from 40–70% can be guaranteed, the primary requirements for indoor materials are high transpirability to water vapour, avoiding the storage of humidity, and the ability to act as an hygroscopic buffer by absorbing and desorbing moisture [35]. The capacity of a finish to

absorb water vapor during exposure at high levels of RH and to release water vapour when the level of RH decreases is expressed as the Moisture-Buffering Capacity (MBC) [36] [37].

This research is aimed at the development and testing of an innovative multi-functional mortar (Italian Patent 102017000033750) for indoor finishes, which is capable of passively improving IAQ, thus benefitting the health and comfort of occupants, in terms of permeability, MBC, de-polluting activity and inhibition of mould growth, besides fulfilling the ordinary requirements. In the developed mix, conventional sand is replaced by volume with biomass ashes and an unconventional aggregate, characterized by high adsorption properties and currently not used in the building sector but, instead, in water/air depuration processes [38]. The interaction with different $TiO_2$ agents activable under UV and VIS radiation [39], as declared in the product's datasheet, is also considered. If $TiO_2$ is present, the unconventional adsorbent aggregates give large contacting areas to the catalytic agent which, thanks to their high specific surface, can potentially improve the de-pollution activity of the material. In this way, saturation of the adsorbent material could also be avoided, providing the benefit of maintaining the same efficiency over time [40]. As references, a traditional mortar and two different commercial pre-mixed products for the same indoor application were manufactured and tested.

## 2. **Experimental program**

### 2.1.**Materials**

A hydraulic lime, classified as LIC 3.0 according to UNI EN 15368:2010, with a density of 2650 kg/m$^3$ (commercial product Plastocem, by Italcementi) was used as binder.

The commercial sand, CA 400 (provided by Cava Gola della Rossa, Italy), was chosen as conventional aggregate for the reference mortar, which is a calcareous sand with 98% purity, and water absorption to reach the saturated surface dry (ssd) condition of 5% in weight and ssd density of 2650 kg/m$^3$.

The aggregates used in the patented mix are a porous adsorbent material and fly/bottom ash obtained from a biomass (corn cobs; USA) thermal plant. The porous adsorbent material is currently not used in the building sector, but in water/air depuration processes [38]. It was obtained in the form of granules about 10 mm in diameter, and its water absorption to reach the ssd condition is 86% with corresponding density of 1310 kg/m$^3$. Before being added into the mix, it was ground and sieved at 300 µm, in order to reach a grain size suitable for indoor finishes.

Fly and bottom biomass ashes are a mixture of inorganic and organic compounds, due to the presence of unburnt components. The water absorption to reach the ssd condition is 49% and 20%, and the ssd density is 1410 and 1940 kg/m$^3$ for fly and bottom ashes, respectively. The ashes were chemically

characterized by X-ray analysis, using an RX Philips PW 1730 X-ray diffractometer (operating voltage/current 40 kV/30 mA; scan mode: continuous speed, 3°/min), and by thermogravimetric differential (TG-DTA) analysis (STA 409 EP) up to a temperature of 1000 °C with a heating rate of 10 °C/min in an oxidizing environment. Ashes were crushed and sieved at 90 µm before the analysis, in order to provide a homogeneous sample.

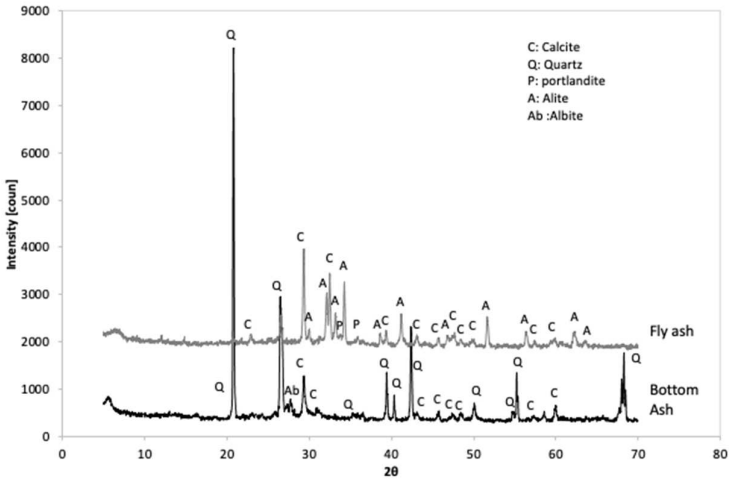


***Figure 1. X-ray diffraction patterns of biomass fly and bottom ashes.***

For both ashes, the most present crystalline phase was quartz, followed by calcium carbonate ($CaCO_3$) (Figure 1). In the case of fly ash, the presence of alite was also detected, as well as traces of calcium hydroxide due to hydration of CaO under environmental humidity. In case of bottom ashes, trace albite was observed. As the presence of amorphous phases gives a curve baseline in the range of 30° [41], no amorphous phases were detected in the current ashes.

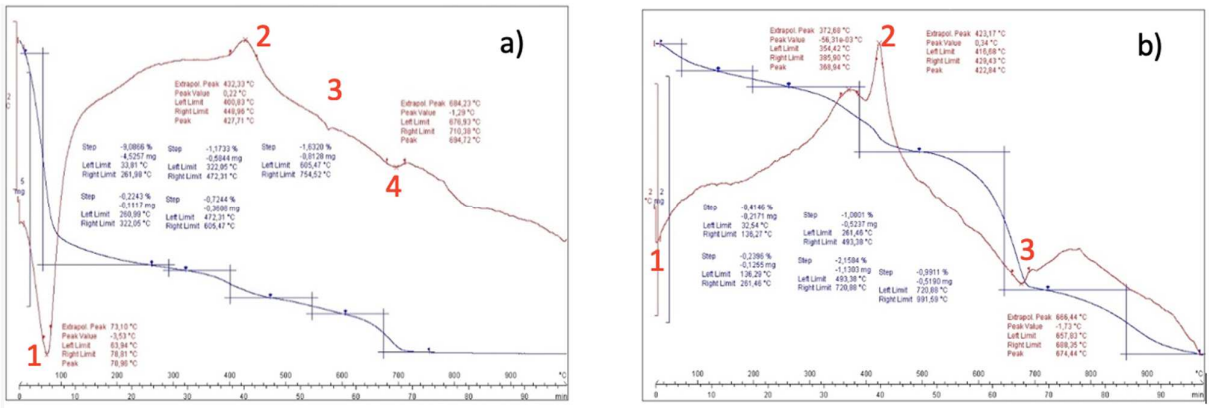


***Figure 2 TG/DTA of fly (a) and bottom ashes (b)***

Calcium carbonate was detected also in TG, as an endothermic peak at T ~ 700 °C (step 4 in Figure 2a; step 3 in Figure 2b), and was quantified as 3.71% and 4.91% of the total weight in fly and bottom ashes, respectively. Moreover, the endothermic peak at T = 80–130 °C (step 1 in Figure 2a, b) was related to the loss of the unbound water. Step 2 in Figure 2a, b, related to an exothermic reaction at T ~ 400 °C, was due to the loss of unburnt organic carbon, quantified as 0.32% and 0.27% of the total weight of fly and bottom ashes, respectively. In fly ash, the presence of $Ca(OH)_2$ was confirmed by the endothermic reaction (labelled step 3 in Figure 2a) from 470 to 650 °C, and quantified as 2.98% of the total weight. Before addition into the proposed mix, the bottom ash was milled and sieved at $d_{max}$ = 500 μm, providing a grain size suitable for indoor finishes.

The effects of three different types of nano-$TiO_2$ on the de-polluting properties of the new finishes was also considered. The selected products were P-25 Aeroxide® by Evonik ($TiO_2$A), KRONOClean 7000 ($TiO_2$K), and KRONOClean 7404 ($TiO_2$J) by KRONOS International Inc., which are activable by VIS radiation. According to the technical data sheet, P-25 is a mixture of anatase–rutile–amorphous phases (78, 14, and 8% in weight, respectively) [42]. The particles had a nano-size of about 20–50 nm. The specific surface, measured by BET, was 35–65 $m^2/g$. The pH of a 4% water dispersion was 3.5–4.5, and the density was reported as 3.1 $g/cm^3$. KRONOClean® is a $TiO_2$ photocatalyst that degrades pollutants both under VIS and UV radiation. As reported in the data sheet, the content of $TiO_2$ is higher than 97.5%, with a prevalence of anatase phase. The particle size is approximately 15 nm. The specific surface area, measured by BET, was higher than 225 $m^2/g$, the density was 2.9 $g/cm^3$, and the pH range of 4–9 in water dispersion, as declared in the technical datasheet. The main difference between the last two photocatalytic products is the carbon content which, for $TiO_2$J, was up to 6.1% when measured by EDAX analysis, as shown in [43] and in TiO2K was 0.7%, measured by means of TGA, evaluated as organic carbon.

Boron salts (from Durga) were added as a biocide admixture, to prevent possible biological attack in some specimens of the new mixes.

Two different commercial inorganic finish pre-mixes (Commercial 1 and Commercial 2), sold for the same indoor application, were selected and tested for further comparison.

### 2.1.1 Mix design

According to a previous work [44], the optimum water to binder ratio to reach the best consistency was evaluated as 0.58. Table 1 provides the mix design parameters of the tested mortars. Aggregate was used in ssd condition; in this state, the aggregate does not absorb or release water in the mix, without any changes to the water to binder ratio (w/b).

185 ***Table 1. Mix design (g/l) of the tested mortars. * KRONOClean 7000 (TiO2K), and **KRONOClean 7404 (TiO2J)***

| Mix | Water | Hy-lime | Sand | Adsorbent | Bottom ash | Fly ash | $TiO_2$ | | Premixed mortar |
|---|---|---|---|---|---|---|---|---|---|
| | | | | | | | P-25 | KronoClean | |
| | *g/l* | *g/l* | *g/l* | *g/l* | *g/l* | *g/l* | *g/l* | *g/l* | *g/l* |
| Reference (REF) | 256 | 437 | 1535 | | | | | | |
| Reference TiO2 (REF TiO2) | 256 | 437 | 1535 | | | | 26 | | |
| Commercial 1 (COM1) | 286 | | | | | | | | 1360 |
| Commercial 2 (COM2) | 408 | | | | | | | | 1360 |
| MIX1 | 256 | 437 | - | 379 | 281 | 204 | | | |
| MIX1 TiO2A | 256 | 437 | - | 379 | 281 | 204 | 26 | | |
| MIX1 TiO2K | 256 | 437 | - | 379 | 281 | 204 | | 26* | |
| MIX1 TiO2J | 256 | 437 | - | 379 | 281 | 204 | | 26** | |

186

187 The two commercial pre-mixes (Commercial 1 and Commercial 2) were prepared by adding the
188 amount of water suggested in the technical data sheets.
189 In presence of biomass ashes, boron salt was added in MIX1, MIX1 $TiO_2$A, and MIX1 $TiO_2$J
190 specimens as a water-based solution (active principle of 16%), at the dosage indicated in the technical
191 data sheet (0.06 g for each litre of cast).

192

193 2.1 **Methods**

194 2.1.1 **Fresh, mechanical, and micro-structural properties**

195 The fresh properties of mortars were evaluated in terms of workability class. The slump was measured
196 with a truncated conical mould and jolting table, according to the standard UNI EN 1015-3:2007.
197 After 28 days of curing at Temperature (T) of 20 ± 2 °C and Relative Humidity (RH) at 95 ± 5% for
198 the first 7 days and 65 ± 5% for the following 21 days, the hardened properties of mortars were
199 investigated. The compressive strength was evaluated, according to the standard UNI EN 1015-

11:2007, in 4 × 4 × 16 cm specimens, by means of a Galdabini hydraulic press with a precision of 1%.

The density of hardened mortars (ρ, in kg/m$^3$) was evaluated by weighing and measuring (with a calliper) the dimensions of the different dried specimens. Specimens were considered dry when, after exposure in an oven at T = 50 °C, two different weights in a time interval of at least 24 hours did not exceed 0.1%.

In hydraulic lime-based materials (as well as cementitious ones), the porosity can be divided as follows: i) gel pores—nanopores from about 0.5 to 10 nm, inside the hydration products; ii) capillary pores—micropores from 10 nm to 5 µm, mainly affected by the degree of hydration and the w/b ratio; iii) macropores—higher than 5 µm, due to the entrainment of microbubbles; and iv) the porosity within the aggregate, which is related to the type of aggregate [34]. The pore size distribution of mortars was studied in the pressure range of 0.01–200 MPa by means of Mercury Intrusion Porosimetry (MIP) using a PASCAL 240 (Thermo Fisher Scientific, Waltham, MA, USA). For each type of mortar, three fragments with dimensions of about 1 cm$^3$ were sampled and tested, and the average results are reported.

### 2.1.2 **Thermo-hygrometric properties**

As reported in a previous study [18], small amounts of $TiO_2$ do not affect the thermo-hygrometric behaviour of mortars. In this case, $TiO_2$ was added at low percentages (2% by solid weight); thus, the thermo-hygrometric properties, in terms of water vapor permeability, Moisture Buffering Capacity (MBC), and thermal conductivity, were tested only for mixes without $TiO_2$.

The water vapor permeability was tested according to UNI EN 1015-19:2007, and data were processed according to UNI EN ISO 12572:2007, which evaluates the water vapor resistance factor (µ) in cylindrical specimens (h = 3 cm, d = 13 cm).

The MBC of finishes was assessed on cylindrical specimens (h = 3 cm, d = 10 cm), by means of a simplified version of the NORDTEST methods [44].

The thermal properties were measured in terms of thermal conductivity, according to UNI EN 12664:2002, at T = 20 ± 2 °C and RH = 50 ± 5%. Equation (1) was used to evaluate the data:

$$\lambda = \frac{Jd}{(T_2 - T_1)^2} \quad (1)$$

where $J$ is the heat flux (W/m$^2$), $d$ is the distance between the thermocouples (m), and $T_1$ and $T_2$ are the temperatures at the two different sides of the sample (K). For each mix, three specimens were tested and the average values are reported.

### 2.1.3 **Inhibition of mould growth test**

Evaluation of the mould growth inhibition effect was performed according to UNI EN 15457:2014 using *Aspergillus niger* (DMS 126) which generally grows in humid indoor environments such as bathrooms, and which can cause health problems including allergies and asthma, especially during prolonged exposure. The methodology for quantification of the inoculum was performed as described in previous works [45][46]. The specimens (5 × 5 × 0.5 cm prisms) were casted and cured for 28 days, as described in Section 2.2.1. After the curing period, the pH of the mortars was tested, in order to ensure that the initial basicity of the mortar was lost, as alkalinity generally inhibits mould growth [46]. To guarantee sterile conditions for the inoculum, the specimens were sterilized in an oven at T = 150 °C for 2 hours. Then, the inoculum was provided on an agar substrate under a laminar flow hood and the specimens were inserted into petri boxes, in order to maintain sterility outside the hood, and incubated at 24°C.

Mould growth was monitored for 28 days under two different conditions: without any irradiance (dark condition) and under visible irradiation for at least 8 hours of exposure per day. As blank tests, three samples of Aspergillus grown on sterile filter paper were provided for each condition of inoculum, to verify the vitality of Aspergillus. Quantification of the inoculum was conducted once a week for 28 days, and the average results of three inocula are reported. To quantify the percentage of colonized area on the surface of the specimens, photos of the specimens were taken and elaborated by means of the ImageJ and GIMP2 software. The results obtained from the inoculum after 28 days are reported and discussed below.

### 2.1.4 **De-polluting properties**

The photocatalytic activity of mortars was assessed according to UNI 11247:2009, which measures the activity of inorganic photocatalytic materials in terms of the degradation rate of nitrogen oxides ($NO_x$) in plug flow condition. The photocatalytic activity (PC) was tested without irradiation (dark) and under both UVA and VIS irradiation and was expressed in terms of the ratio of mineralized NO over total $NO_x$ flux directed in a plug flow reactor. The $NO_x$ flux was provided by a tank at 500 ppb ± 5 NO (SAPIO S.r.l., Monza, Italy), kept constant by mixing with air at T = 25 °C and RH 50 ± 10% using a dilution system (Calibrator 8188, Rancon Instruments S.p.A., Milan, Italy). In the outlet flux, the concentrations of NO and $NO_2$ were continuously monitored using a chemiluminescence $NO_x$ analyser (nitrogen oxide analyzer model 8841; Monitor Labs, Englewood, CO, United States). According to the standard, the borosilicate glass photoreactor had a volume of 3 litres and the specimen (cylinder with d = 8 cm and h = 0.8 cm) was placed in the centre. Then, 20 W/m$^2$ UVA irradiance, measured by a photo-radiometer (Delta Ohm, HD2102.2, Padua, Italy, equipped with LP471 probe), was provided using a UV 300 W metal halogen lamp, placed 25 cm from the surface

of the specimen outside the reactor. VIS light was provided by placing an UV screen protector between the lamp and the reactor. Irradiation of the sample was guaranteed until stable conditions were reached (usually 30 min).

The de-polluting property regarding VOCs adsorption was evaluated by means of batch tests, where the VOCs concentration decay was measured over time using a Gas Chromatographer (GC-Carlo Erba Gas 8000 Top). Tests were conducted in dark conditions, and under UV and VIS radiation, in order to evaluate the possible photocatalytic activity. Under UVA radiation, an irradiance of 10 $W/m^2$—as measured by a photo-radiometer (Delta Ohm, HD2102.2, Padua, Italy, equipped with LP471 probe)—was provided by a 9 W UV-A lamp (Philips); whereas, for VIS radiation, a 9 W lamp was used (Osram). The de-pollution test was performed on cylindrical specimens (h = 0.8 cm, d = 8 cm) following the procedure described in [46], for a total exposed surface of 50 $cm^2$. Methyl ethyl ketone (MEK) was used as a model pollutant, injected into a borosilicate glass box where the specimen was inserted before. MEK concentration was assessed each 10 minutes for 120 minutes. A pseudo-second-order (PSO) [47] adsorption kinetic model was used to describe the adsorption kinetics of MEK into the specimen, as described by the following equation:

$$q_t = q_e(1 - e^{-k_1 t}) \quad (2)$$

where $q_t$ and $q_e$ ($mg/cm^2$) are the adsorptive removal capacity at equilibrium and a specific time (t), respectively, normalized on the sample surface; and $k_1$ is the adsorption rate constant. The difference between the initial MEK concentration without specimen (C0, equal to 2402 $mg/m^3$) and the concentration monitored over the time (Ci) was used to determine $q_t$. The test was repeated at least three times, and was directly fitted to Equation 2.

## 3 Results and Discussion

### 3.1 **Fresh, mechanical, and micro-structural properties**

All the prepared mortars were classified as stiff, according to UNI EN 1015-6:2007.

The compressive strength, density, and accessible porosity results, evaluated after 28 days of curing, are reported in Figure 3. Both commercial and new mortars had lower compressive strength than the reference mortar. In the case of COM1 and COM2, the compressive strength values were 5% and 55% lower than reference mortars, respectively (Figure 3a). MIX1 (with and without $TiO_2$) showed a decrease in compressive strength of about 25% (when compared to reference mortar) or 20% (when compared to COM2). The reduction of compressive strength in the proposed mix was due to the addition of the very porous adsorbent aggregate [44], even if the addition of biomass ashes facilitated partial recovery of the mechanical resistance loss, thanks to their pozzolanic activity [48][49][50,51].

The presence of alite in the ashes, as detected by XRD (Figure1), would favour the formation of calcium silicate hydrates in the binding phase, thus enhancing the mechanical performance. As expected, the mechanical behaviour was not significantly changed with the addition of $TiO_2$.

According to UNI EN 998-1:2010, the maximum value of density for indoor mortar to be classified as lightweight is 1300 kg/m$^3$. As the highly porous adsorbent aggregate and biomass ashes have lower density than conventional sand, the obtained mortars were lighter than the reference and both commercial mortars. As reported in Figure 3b, MIX1 and COM1, classified as lightweight mortars, and the new mortar had lower density than the commercial products and the reference mortars, by about 15% and 35%, respectively, regardless of $TiO_2$ presence.

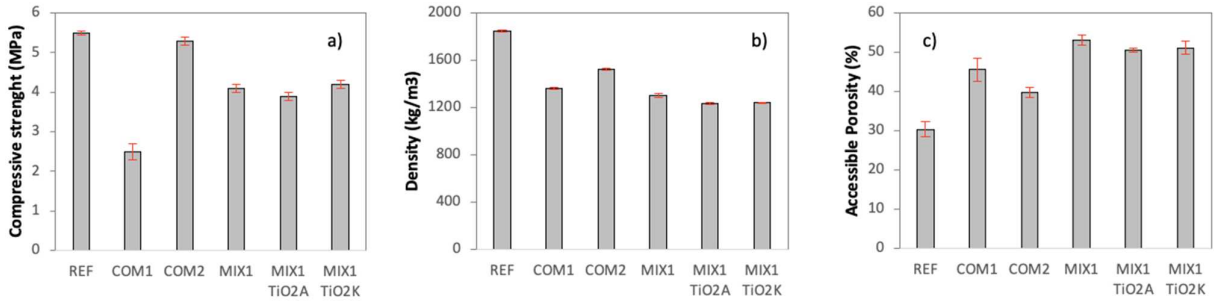


***Figure 3. Compressive strength (a), density (b), and accessible open porosity (c).***

Accessible open porosity was evaluated by MIP (Figure 3c), and both the relative and cumulative pore volume distribution curves are shown in Figure 4. The REF mortar had the lowest total porosity. COM1 and COM2 had 10% and 15% higher total porosity than REF, respectively, whereas the new mortar showed the highest value of total porosity (again, regardless of $TiO_2$ addition). Furthermore, the pore size distribution was not significantly affected by the type or the presence of $TiO_2$, as shown in Figure 4, in which the pore distribution curves of reference, commercial, and multi-functional mortars are compared. REF and commercial mortars present unimodal distributions, whereas the new mortar shows a bi-modal distribution. The main factor usually affecting the porosity of the matrix is the type of binder. In hydraulic lime mortar, the pore diameter threshold—which is the first inflection point of the curve—generally ranges from 1 to 3 µm; that is, hydraulic lime introduces a higher medium-pore size porosity into the matrix than cement [20]. In this case, the REF mortar had a modal pore diameter of 0.93 µm and a threshold pore diameter of 1.54 µm; while COM1 and COM2 had modal diameters of 1.60 µm and 0.90 µm and threshold pore diameters of 3.27 µm and 1.20 µm, respectively. Regardless of the type of $TiO_2$, the unconventional mortars all had the first peak at 1.2 µm, except for M1 $TiO_2$A, which was at 0.93 µm. The second peak, at a lower pore diameter, was at 0.04 µm for M1 and M1 $TiO_2$A, and 0.04 µm and 0.021 µm for the mortars with titanium dioxides.

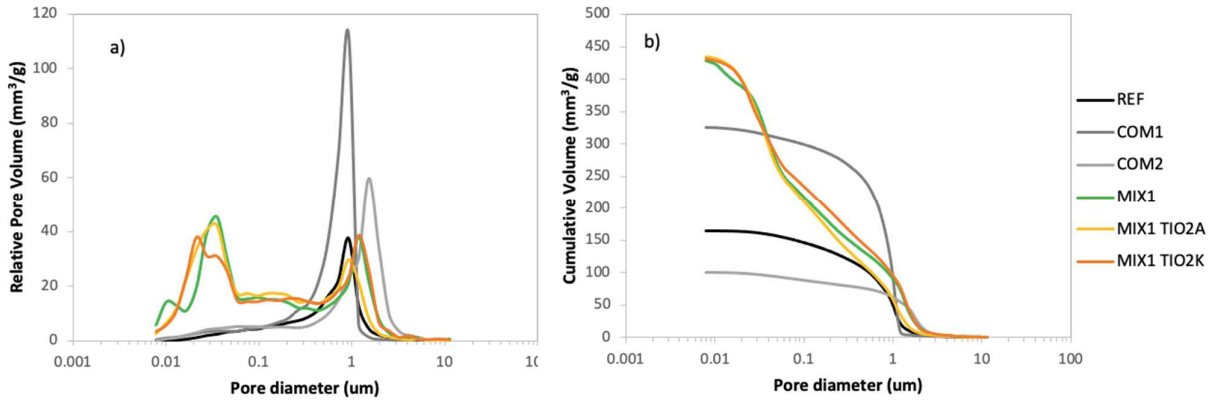


***Figure 4 Relative (a) and cumulative (b) pore volume distribution of different mortars***

## 3.2 Thermo-hygrometric properties

As the influence of $TiO_2$ on hygro-thermal behaviour of mortars at low percentages has been reported to be negligible [18], only mortars without $TiO_2$ were tested for thermo-hygrometric properties. The obtained results, with relative standard deviations, are reported in Table 2.

***Table 2. Thermo-hygrometric properties of mortars: water vapor resistance factor, moisture buffering value, and thermal conductivity.***

| Mix | μ | s.d.* | MBV | s.d.* | λ | s.d.* |
|---|---|---|---|---|---|---|
| | (-) | (-) | (g/m²*RH%) | (-) | (W/mK) | (-) |
| REF | 19.8 | 1.2 | 0.15 | 0.01 | 0.124 | 0.016 |
| COM1 | 14.0 | 0.2 | 0.30 | 0.05 | 0.096 | 0.001 |
| COM2 | 15.8 | 0.9 | 0.25 | 0.01 | 0.101 | 0.004 |
| MIX1 | 11.4 | 0.2 | 0.61 | 0.18 | 0.083 | 0.001 |

s.d. standard deviation

Low μ factor values indicate high permeability. REF mortar showed the highest μ values and, therefore, lower water vapor permeability. Commercial mortars had a μ value lower than that of the REF mortar: of about 20% for COM1 and 30% for COM2. M1 had the lowest value of μ—40% lower than REF and about 20 and 25% lower than COM1 and COM2 mortar—and, therefore, the highest water vapor permeability. Taking into account that the same hydraulic binder was used for all the tested mortars, the differences were mainly due to the different porosities of aggregates. In particular,

the results follow the well-known principle in which a higher pore threshold radius (Figure 4) leads to higher transpirability [34] [52] . The total amount of porosity is also very influential on permeability: in the case of M1, the higher volume of pores, in terms of total porosity (Figure 3c), led to a lower hygroscopic resistance factor, as reported in Figure 5a.

The interaction between mortars and the indoor RH was also studied, by measuring the change in moisture content of specimens (Δm) exposed at different RHs. Table 2 shows Δm normalized on the surface of specimens, representing the MBV values. The REF mortar had the lowest ability to exchange water vapor and, consequently, the lowest MBV. Both commercial mortars had a higher capacity to exchange water vapor than the REF mortar, about 100% and 75% for COM1 and COM2, respectively. The unconventional mortar had up to three times higher MBV, compared to the reference mortar. Furthermore, in this case, the result was strictly related to the porosity of the mortar, as a higher total volume of pores implies a higher available mortar surface with large pore volume, providing sufficient space for the adsorbate (in this case, water) to be trapped in [53]. The obtained results confirmed that the higher the accessible porosity, the higher the MBV value (Figure 5b); unconventional mortars had the highest total porosity (Figure 3c) and, therefore, the highest MBV values (Table 2). Moreover, higher permeability usually indicates higher water vapor-exchanging ability [54] [55].

Concerning the ability of the materials to contribute to wall system insulation [53], the REF mortar had the highest thermal conductivity, while commercial mortars both had about 20% lower thermal conductivity values than the reference mortar. MIX1 had the lowest value: 35% lower than the REF and about 20% lower than COM 1 and COM 2. Furthermore, in the case of thermal conductivity, the higher the porosity, the lower the thermal conductivity; with a good linear correlation, as shown in Figure 5c.

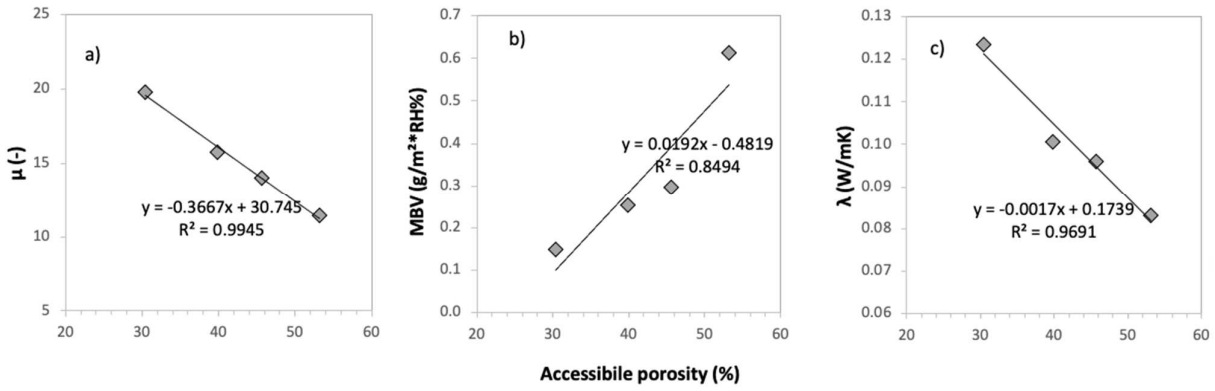


***Figure 5. Relationships between accessible porosity and water vapor permeability factor (a), moisture buffering value (b), and thermal conductivity (c).***

### 3.3 Inhibition of mould growth test

REF mortar had the highest resistance to the biological attack under both test conditions [46], as shown in Figure 6, probably due to the absence of any nutrient on the mortar surface (e.g., organic carbon or potassium). P-25 was chosen as benchmark $TiO_2$ (TiO2A) and KRONOClean 7404 (TiO2J) was tested, due to the high presence of organic carbon [43], which creates favourable environmental conditions, in terms of mould growth. Commercial mortars were not tested, as their datasheets have already reported their mould growth inhibition ability.

All M1 mortars (without and with $TiO_2$) were unable to completely inhibit the growth of micro-organisms on their surfaces. The main reasons for this could be the presence of biomass ash, which favours mould growth, as well as the roughness of the surface [56]. The high accessible porosity of the M1, as reported in Figure 3c, also assists in the capillary uptake of the agar nutrient in the mortar, providing a better substrate for mould growth, when compared to REF.

The presence of inactivated $TiO_2$ (under dark condition) increased the susceptibility of mortars to biological attack, with an enhancement in the colonized area up to 6 and 10 times for $TiO_2$A and $TiO_2$J, respectively, when compared to M1 without $TiO_2$. This was probably due to the hydrophilicity of $TiO_2$: the test was conducted in dark, but the inoculum was provided under VIS radiation, which could be enough to activate the photo-induced hydrophilicity [57][58][44]. In the case of $TiO_2$J, the higher biological attack could be due to the higher content of the organic carbon [43], which provides additional nutrients for the growth of mould.

Therefore, surface treatment of the materials should be considered necessary to prevent biological attack [59] when the control of environmental factors (e.g., irradiation, composition of the material, and humidity) cannot be guaranteed [60]. In this case, the addition of boron salt (SB) relevantly decreased mould growth under dark conditions. In the case of M1 $TiO_2$A, the colonized area decreased from 33 to 7% and, in the case of M1 $TiO_2$J, it decreased from 54 to 15%. When specimens were prepared with both $TiO_2$ and boron salt and tested under VIS conditions, the colonized area became negligible, showing that the well-known antibacterial ability of activated $TiO_2$ under UV assists the biocidal action of the boron salts [61][62] [63].

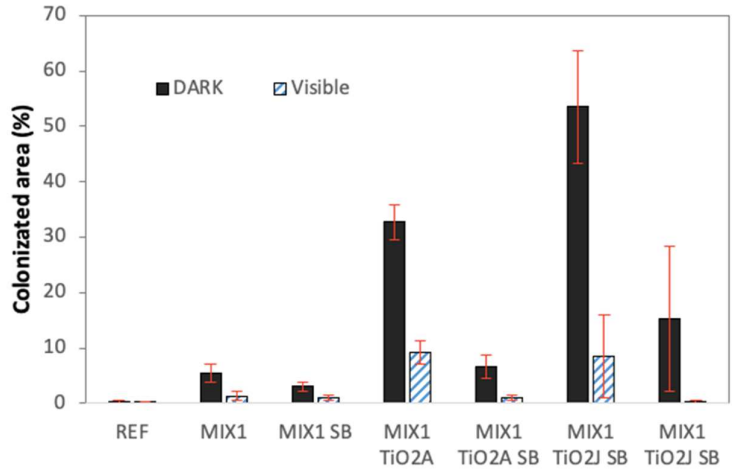


***Figure 6. Percentage of colonized area.***

### 3.4 **De-polluting properties**

As expected, NO decomposed only in the presence of $TiO_2$, as shown by the NOx abatement factor and the $NO_2$/NO removal results reported in Figure 7. The values lower than 5% detected in REF, COM1, and MIX 1 under UV radiation were considered negligible.

The removal of up to 6% of NO in the reference sample was ascribed to photolysis of the pollutant, and to the sorption and conversion of NO into nitrous acid [64][65].

In the case of commercial mortars, the presence of $TiO_2$ was declared for COM2, and 18% NOx removal was assessed under UV radiation. The abatement was detected also under VIS radiation, but only at a negligible percentage (8%).

Both types of $TiO_2$ enhanced the photocatalytic degradation of M1 mortar: up to 30% under UV irradiation. The photocatalytic efficiency was also demonstrated under VIS radiation, but with lower values (of about 18% and 7% for $TiO_2$A and $TiO_2$K, respectively).

The ratio between $NO_2$ and NO was also considered: the higher the ratio, the higher the production of unwanted $NO_2$ during the reaction. Figure 7b shows that the production of unwanted $NO_2$ was negligible for all the mortars. For M1 mortars, with adsorbent materials as unconventional aggregate, this can be ascribed to the synergistic effect between adsorption and photocatalysis, as has already been detailed in previous studies [66][67]. The enhanced reactivity with Ti-OH by $NO_2$ disproportion is due to the higher amount of water adsorbed in the proximity of $TiO_2$ [68] and the consequent reaction of $NO_x$ with alkaline products [53]. Additionally, the pore structure of MIX 1 with the addition of $TiO_2$ enhanced the photocatalytic effect [69]. These pores act as a booster for photocatalytic activity, as has been stated in [70], in cement mortars with $TiO_2$. These authors concluded that the formation of capillary pores in the range of 0.01–0.05 μm was critical for the

enhancement of the photocatalytic activity (NO abatement), which has also been demonstrated in [71], where higher NO degradation was detected in specimens with outstanding increase in capillary pores.

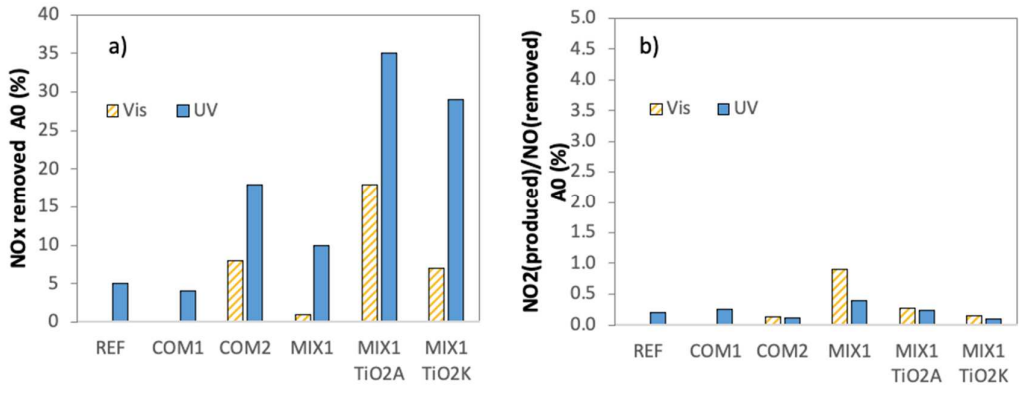


***Figure 7. Percentage of $NO_x$ removed (a), and ratio between $NO_2$ produced and NO removed (b) during plug-flow test.***

During the VOCs de-polluting capacity test, the specimen was sealed inside a box, into which a known quantity of the model pollutant MEK was injected. Then, the MEK residual concentration was monitored for 120 mins. The MEK concentrations at the end of the tests are shown in Figure 8.

The commercial products COM1 and COM2 showed 20% higher and 20% lower de-polluting properties than REF mortar, respectively. M1 mortar showed a de-polluting capacity about 40% higher than the REF mortar and both COM mortars. After 2 hours of the test, the residual MEK in the box was only 20% when a M1 finish was used [38]. The addition, both types of $TiO_2$ did not significantly influence the de-polluting capacity under dark conditions. Under VIS radiation, the effect of $TiO_2K$ was not observed; whereas, under UV radiation, the percentage of residual MEK inside the box ranged from 11–22%. $TiO_2A$ provided negligible (about 4%) enhancements in de-polluting capacity under both visible and UV radiation.

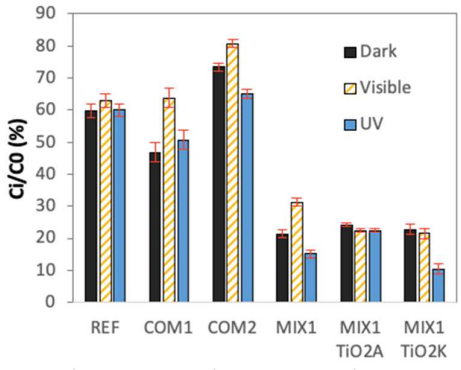

***Figure 8. Residual concentration inside the box after 120 min of monitoring.***

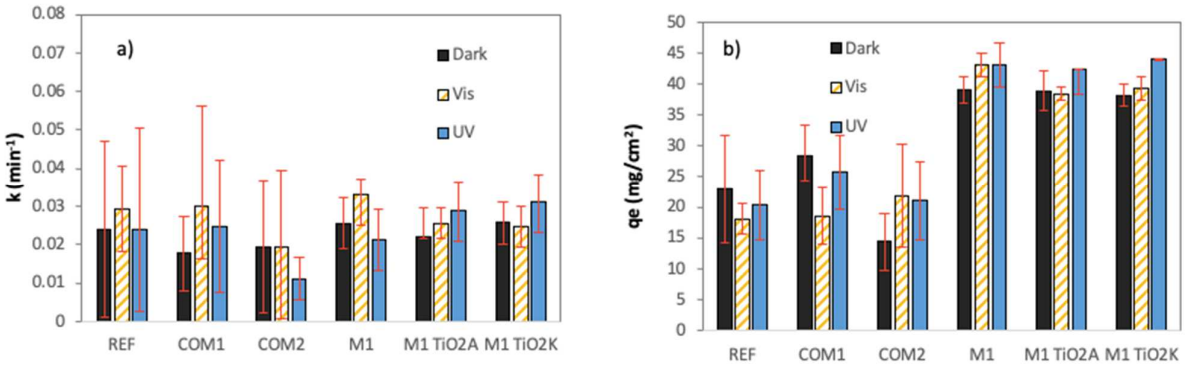


***Figure 9. Adsorption rate constant $k_1$ a) and the adsorption rate constant and specific MEK removal capacity at equilibrium $q_e$ b).***

The unconventional aggregates added in M1 cause the adsorption process to be predominant over the PCO, even under visible and UV radiation, as has been shown in [72]. In fact, when the monitored residual concentration data were represented in terms of adsorption kinetics, in terms of constant adsorption rate, the results could be classified in two groups with similar values (Figure 9a): one related to the M1 mortars with adsorbent unconventional aggregate, and the other to the REF and COM mortars. High errors bars occurred during the elaboration of the data for REF, COM1, and COM2, as well as when the specific MEK removal capacity at equilibrium $q_e$ was calculated (Figure 9b), highlighting that no significant adsorption mechanism was present in those specimens [73]. On the other hand, MIX1, MIX1 $TiO_2$A, and MIX1 $TiO_2$K had higher MEK removal capacities (approx. 30%) than REF and COM mortars, and the test conditions (UV, VIS, or dark) did not affect the adsorbent properties.

The adsorption efficiency of the finish was extremely enhanced when the adsorbent aggregate was used and, consequently, a high specific surface interacted with the environment. Moreover, with a higher pore size reduction, a higher de-polluting capacity was observed [71], with good linear correlation, as reported in Figure 10.

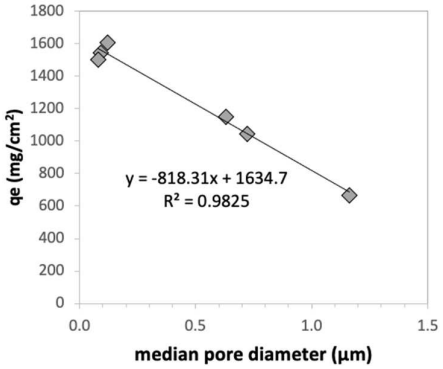

*Figure 10. De-polluting properties, in terms of specific MEK removal capacity at equilibrium $q_e$ under dark conditions.*

The de-polluting property was higher in M1 mortars than REF and COM mortars, due to the combination of the adsorbent process and PCO. The photocatalyst activity can be enhanced with a high presence of micro–nano-pores [74]: the larger the volume of pores with diameter higher than 80 nm, the higher the PCO efficiency [19]. Therefore, the high porosity of M1 mortars allowed for the absorption of pollutants into their internal structure [22]. Moreover, during the test, STD and COM mortars were close to reaching saturation conditions, while the new mortars continued to adsorb and decompose the loaded MEK, as has been detailed in [46].

## 4 Conclusions

An unconventional mortar for use as an indoor finish was designed, characterized, and compared to a traditional reference mortar and two commercial pre-mixes for the same application. In the new finish mortar, an unconventional aggregate—based on an adsorbent material which is generally not used in the building sector, but in air/water purification processes—was adopted, instead of traditional sand. The patented new finish has potentially high sustainability, thanks to the use of hydraulic lime and biomass wastes, instead of cement and conventional aggregates.

The innovative mix was able to fulfil all traditional requirements for an indoor finish. The new mortar can be classified as a lightweight mortar ($\rho < 1300$ kg/m$^3$), with density 30% lower than the REF mortar and around 10% lower than COM mortars. This low density was due to the use of unconventional lightweight adsorbent aggregates, which also led to 20%, 10%, and 5% higher porosity, when compared to the REF, COM1, and COM2 mortars, respectively.

Regardless of the high porosity and low density, only a 5% decrease in compressive strength, with respect to the REF mortar, was detected; as such, the proposed mortar can be considered acceptable for the proposed application. Compared to commercial products, the compressive strength was 5% lower or around double, according to the type of mortar. The new formulation had thermal conductivity 35% lower than that of the REF mortar and about 20% lower than those of commercial mortars; as well as the lowest water vapor resistance factor (about 40% lower than REF and about 20 and 25% lower than the COM mortars). This ensures the highest transpirability, preventing the stagnation of water vapour.

In terms of moisture buffering capacity, the best performance was also detected in the new mortar, with three times higher MBV than the reference mortar and the double and 75% higher, when compared to the respective COM mortars.

Concerning the de-polluting ability, the patented finish reached the NOx abatement of 35%, 75% higher than COM mortar with the addition of $TiO_2$ activated under UV radiation, whereas the adsorbent properties were enhanced by 50% with respect to REF and both commercial mortars. Finally, the behaviour of the innovative mortar, in terms of biological attack, was improved when a biocide was added into the mix.

## Patent

***Italian Patent 102017000033750***


## Acknowledgements

The authors wish to thank EVONIK and KRONOS, which kindly supplied titanium dioxides. The co-grant for research contract was provided thanks to the program 'FSE-REACT-EU, PON Ricerca e Innovazione 2014-2020 DM 1062/2021'.


## References


[1] Q. Chen, H. Feng, B. Garcia de Soto, Revamping construction supply chain processes with circular economy strategies: A systematic literature review, J. Clean. Prod. 335 (2022) 130240. doi:10.1016/j.jclepro.2021.130240.

[2] European Commission, The European Green Deal, (2019). doi:10.1017/CBO9781107415324.004.

[3] S.E. Frey, H. Destaillats, S. Cohn, S. Ahrentzen, M.P. Fraser, The effects of an energy efficiency retrofit on indoor air quality, Indoor Air. 25 (2015) 210–219. doi:https://doi.org/10.1111/ina.12134.

[4] P. Wolkoff, Indoor air humidity, air quality, and health – An overview, Int. J. Hyg. Environ. Health. 221 (2018) 376–390. doi:10.1016/j.ijheh.2018.01.015.

[5] Y. Al horr, M. Arif, M. Katafygiotou, A. Mazroei, A. Kaushik, E. Elsarrag, Impact of indoor environmental quality on occupant well-being and comfort: A review of the literature, Int. J. Sustain. Built Environ. 5 (2016) 1–11. doi:10.1016/j.ijsbe.2016.03.006.

[6] WHO, Development of WHO Guidelines for Indoor Air Quality - Report on a Working Group Meeting, World Heal. Organ. Reg. Off. Eur. (2006) 1–27. http://www.euro.who.int/__data/assets/pdf_file/0007/78613/AIQIAQ_mtgrep_Bonn_Oct06.pdf.

[7] T. Verdier, M. Coutand, A. Bertron, C. Roques, A review of indoor microbial growth across building materials and sampling and analysis methods, Build. Environ. 80 (2014) 136–149.

539 doi:10.1016/j.buildenv.2014.05.030.
540 [8] M. Pierpaoli, C. Giosuè, M.L. Ruello, G. Fava, Appraisal of a hybrid air cleaning process,
541 Environ. Sci. Pollut. Res. 24 (2017) 12638–12645. doi:10.1007/s11356-016-7880-x.
542 [9] B. Krejcirikova, J. Kolarik, P. Wargocki, The effects of cement-based and cement-ash-based
543 mortar slabs on indoor air quality, Build. Environ. 135 (2018) 213–223.
544 doi:10.1016/j.buildenv.2018.03.011.
545 [10] Kunkel D., E. Gall, J.A. Siegel, A. Novoselac, G.C. Morrison, R.L. Corsi, Passive reduction
546 of human exposure to indoor ozone, Build. Environ. 45 (2010) 445–452.
547 [11] J. Xiong, P. Zhang, S. Huang, Y. Zhang, Comprehensive influence of environmental factors
548 on the emission rate of formaldehyde and VOCs in building materials: Correlation
549 development and exposure assessment, Environ. Res. 151 (2016) 734–741.
550 doi:10.1016/j.envres.2016.09.003.
551 [12] A.D. Tran Le, J.S. Zhang, Z. Liu, D. Samri, T. Langlet, Modeling the similarity and the
552 potential of toluene and moisture buffering capacities of hemp concrete on IAQ and thermal
553 comfort, Build. Environ. 188 (2021) 107455. doi:10.1016/j.buildenv.2020.107455.
554 [13] A.H. Mamaghani, F. Haghighat, C.S. Lee, Photocatalytic oxidation technology for indoor
555 environment air purification: The state-of-the-art, Appl. Catal. B Environ. 203 (2017) 247–
556 269. doi:10.1016/j.apcatb.2016.10.037.
557 [14] L. Senff, D.M. Tobaldi, S. Lucas, D. Hotza, V.M. Ferreira, J.A. Labrincha, Formulation of
558 mortars with nano-SiO2 and nano-TiO2 for degradation of pollutants in buildings, Compos.
559 Part B. 44 (2013) 40–47. doi:10.1016/j.compositesb.2012.07.022.
560 [15] A. Fujishima, X. Zhang, D.A. Tryk, TiO2 photocatalysis and related surface phenomena,
561 Surf. Sci. Rep. 63 (2008) 515–582. doi:10.1016/j.surfrep.2008.10.001.
562 [16] Q.L. Yu, M.M. Ballari, H.J.H. Brouwers, Indoor air purification using heterogeneous
563 photocatalytic oxidation. Part II: Kinetic study, Appl. Catal. B Environ. 99 (2010) 58–65.
564 doi:10.1016/j.apcatb.2010.05.032.
565 [17] S. Lorencik, Q.L. Yu, H.J.H. Brouwers, Design and performance evaluation of the functional
566 coating for air purification under indoor conditions, Appl. Catal. B Environ. 168–169 (2015)
567 77–86. doi:10.1016/j.apcatb.2014.12.012.
568 [18] C. Giosuè, Q.L. Yu, M.L. Ruello, F. Tittarelli, H.J.H. Brouwers, Effect of pore structure on
569 the performance of photocatalytic lightweight lime-based finishing mortar, Constr. Build.
570 Mater. 171 (2018). doi:10.1016/j.conbuildmat.2018.03.106.
571 [19] R. Sugrañez, J.I. Álvarez, M. Cruz-yusta, I. Mármol, J. Morales, J. Vila, L. Sánchez,
572 Enhanced photocatalytic degradation of NOx gases by regulating the microstructure of

mortar cement modified with titanium dioxide, Build. Environ. 69 (2013) 55–63. doi:10.1016/j.buildenv.2013.07.014.
[20] C. Giosuè, Q.L. Yu, M.L. Ruello, F. Tittarelli, H.J.H. Brouwers, Effect of pore structure on the performance of photocatalytic lightweight lime-based finishing mortar, Constr. Build. Mater. 171 (2018) 232–242. doi:10.1016/j.conbuildmat.2018.03.106.
[21] L. Barcelo, J. Kline, G. Walenta, E. Gartner, Cement and carbon emissions, Mater. Struct. 47 (2013) 1055–1065. doi:10.1617/s11527-013-0114-5.
[22] S.S. Lucas, V.M. Ferreira, J.L.B. De Aguiar, Incorporation of titanium dioxide nanoparticles in mortars — Influence of microstructure in the hardened state properties and photocatalytic activity, Cem. Concr. Res. 43 (2013) 112–120. doi:10.1016/j.cemconres.2012.09.007.
[23] I. Karatasios, M.S. Katsiotis, V. Likodimos, A.I. Kontos, G. Papavassiliou, P. Falaras, V. Kilikoglou, Photo-induced carbonation of lime-TiO2 mortars, Appl. Catal. B Environ. 95 (2010) 78–86. doi:10.1016/j.apcatb.2009.12.011.
[24] J. Torkaman, A. Ashori, A. Sadr Momtazi, Using wood fiber waste, rice husk ash, and limestone powder waste as cement replacement materials for lightweight concrete blocks, Constr. Build. Mater. 50 (2014) 432–436. doi:10.1016/j.conbuildmat.2013.09.044.
[25] E. Benhelal, E. Shamsaei, M.I. Rashid, Challenges against CO2 abatement strategies in cement industry: A review, J. Environ. Sci. (China). 104 (2021) 84–101. doi:10.1016/j.jes.2020.11.020.
[26] B.S. Thomas, J. Yang, K.H. Mo, J.A. Abdalla, R.A. Hawileh, E. Ariyachandra, Biomass ashes from agricultural wastes as supplementary cementitious materials or aggregate replacement in cement/geopolymer concrete: A comprehensive review, J. Build. Eng. 40 (2021). doi:10.1016/j.jobe.2021.102332.
[27] E.R. Teixeira, R. Mateus, A.F. Camões, L. Bragança, F.G. Branco, Comparative environmental life-cycle analysis of concretes using biomass and coal fly ashes as partial cement replacement material, J. Clean. Prod. 112 (2016) 2221–2230. doi:10.1016/j.jclepro.2015.09.124.
[28] R. Barbosa, N. Lapa, D. Dias, B. Mendes, Concretes containing biomass ashes: Mechanical, chemical, and ecotoxic performances, Constr. Build. Mater. 48 (2013) 457–463. doi:10.1016/j.conbuildmat.2013.07.031.
[29] S. Maschio, G. Tonello, L. Piani, E. Furlani, Fly and bottom ashes from biomass combustion as cement replacing components in mortars production: Rheological behaviour of the pastes and materials compression strength, Chemosphere. 85 (2011) 666–671. doi:10.1016/j.chemosphere.2011.06.070.

607 [30] J. Shen, Z. Gao, Ozone removal on building material surface: A literature review, Build.
608 Environ. 134 (2018) 205–217. doi:10.1016/j.buildenv.2018.02.046.
609 [31] C. Giosuè, A. Mobili, G. Toscano, M.L. Ruello, F. Tittarelli, Effect of Biomass Waste
610 Materials as Unconventional Aggregates in Multifunctional Mortars for Indoor Application,
611 Procedia Eng. 161 (2016) 655–659. doi:10.1016/j.proeng.2016.08.724.
612 [32] I. Carević, A. Baričević, N. Štirmer, J. Šantek Bajto, Correlation between physical and
613 chemical properties of wood biomass ash and cement composites performances, Constr.
614 Build. Mater. 256 (2020). doi:10.1016/j.conbuildmat.2020.119450.
615 [33] L. Świerczek, B.M. Cieślik, P. Konieczka, The potential of raw sewage sludge in
616 construction industry – A review, J. Clean. Prod. 200 (2018) 342–356.
617 doi:10.1016/j.jclepro.2018.07.188.
618 [34] J. Rissanen, C. Giosué, K. Ohenoja, P. Kinnunen, M. Marcellini, M. Letizia Ruello, F.
619 Tittarelli, M. Illikainen, The effect of peat and wood fly ash on the porosity of mortar,
620 Constr. Build. Mater. 223 (2019). doi:10.1016/j.conbuildmat.2019.06.228.
621 [35] H.J. Kim, S.S. Kim, Y.G. Lee, K.D. Song, The hygric performances of moisture
622 adsorbing/desorbing building materials, Aerosol Air Qual. Res. 10 (2010) 625–634.
623 doi:10.4209/aaqr.2010.08.0070.
624 [36] B.K. Kreiger, W. V. Srubar, Moisture buffering in buildings: A review of experimental and
625 numerical methods, Energy Build. 202 (2019) 109394. doi:10.1016/j.enbuild.2019.109394.
626 [37] C. Rode, R. Peuhkuri, B. Time, K. Svennberg, T. Ojanen, P. Mukhopadhyaya, M. Kumaran,
627 S.W. Dean, Moisture Buffer Value of Materials in Building, J. ASTM Int. 4 (2007) 1–12.
628 doi:10.1520/JAI100369.
629 [38] F. Tittarelli, C. Giosuè, A. Mobili, M.L. Ruello, Influence of binders and aggregates on
630 VOCs adsorption and moisture buffering activity of mortars for indoor applications, Cem.
631 Concr. Compos. 57 (2015) 75–83. doi:10.1016/j.cemconcomp.2014.11.013.
632 [39] N. Todorova, T. Giannakopoulou, S. Karapati, D. Petridis, T. Vaimakis, C. Trapalis,
633 Composite TiO2/clays materials for photocatalytic NOx oxidation, Appl. Surf. Sci. 319
634 (2014) 113–120. doi:10.1016/j.apsusc.2014.07.020.
635 [40] A.H. Aïssa, E. Puzenat, A. Plassais, J.-M. Herrmann, C. Haehnel, C. Guillard,
636 Characterization and photocatalytic performance in air of cementitious materials containing
637 TiO2. Case study of formaldehyde removal, Appl. Catal. B Environ. 107 (2011) 1–8.
638 doi:10.1016/j.apcatb.2011.06.012.
639 [41] D. Eliche-Quesada, A. Calero-Rodríguez, E. Bonet-Martínez, L. Pérez-Villarejo, P.J.
640 Sánchez-Soto, Geopolymers made from metakaolin sources, partially replaced by Spanish

641 clays and biomass bottom ash, J. Build. Eng. 40 (2021). doi:10.1016/j.jobe.2021.102761.
642 [42] M. Pierpaoli, O. Favoni, G. Fava, M.L. Ruello, A novel method for the combined
643 photocatalytic activity determination and bandgap estimation ., Methods Protoc. 1 (2018) 1–
644 12. doi:https://doi.org/10.3390/mps1020022.
645 [43] Q. Maqbool, N. Czerwinska, C. Giosuè, S. Sabbatini, M.L. Ruello, F. Tittarelli, New waste-
646 derived TiO2 nanoparticles as a potential photocatalytic additive for lime based indoor
647 finishings, J. Clean. Prod. 373 (2022) 133853. doi:10.1016/j.jclepro.2022.133853.
648 [44] C. Giosuè, M. Pierpaoli, A. Mobili, M.L. Ruello, F. Tittarelli, Influence of Binders and
649 Lightweight Aggregates on the Properties of Cementitious Mortars: From Traditional
650 Requirements to Indoor Air Quality Improvement, Materials (Basel). 10 (2017) 978.
651 doi:10.3390/ma10080978.
652 [45] C. Giosuè, A. Belli, A. Mobili, B. Citterio, F. Biavasco, M.L. Ruello, F. Tittarelli, Improving
653 the Impact of Commercial Paint on Indoor Air Quality by Using Highly Porous Fillers,
654 Buildings. 7 (2017) 110. doi:10.3390/buildings7040110.
655 [46] C. Giosuè, A. Mobili, B. Citterio, F. Biavasco, M.L. Ruello, F. Tittarelli, Innovative
656 hydraulic lime-based finishes with unconventional aggregates and TiO2 for the improvement
657 of indoor air quality, Manuf. Rev. 7 (2020) 1–9.
658 [47] M. Kostoglou, T.D. Karapantsios, Why Is the Linearized Form of Pseudo-Second Order
659 Adsorption Kinetic Model So Successful in Fitting Batch Adsorption Experimental Data?,
660 Colloids and Interfaces. 6 (2022) 55. doi:10.3390/colloids6040055.
661 [48] V. Sata, J. Tangpagasit, C. Jaturapitakkul, P. Chindaprasirt, Effect of W/B ratios on
662 pozzolanic reaction of biomass ashes in Portland cement matrix, Cem. Concr. Compos. 34
663 (2012) 94–100. doi:10.1016/j.cemconcomp.2011.09.003.
664 [49] S. Demis, J.G. Tapali, V.G. Papadakis, An investigation of the effectiveness of the utilization
665 of biomass ashes as pozzolanic materials, Constr. Build. Mater. 68 (2014) 291–300.
666 doi:10.1016/j.conbuildmat.2014.06.071.
667 [50] J. Fořt, J. Šál, R. Ševčík, M. Doleželová, M. Keppert, M. Jerman, M. Záleská, V. Stehel, R.
668 Černý, Biomass fly ash as an alternative to coal fly ash in blended cements: Functional
669 aspects, Constr. Build. Mater. 271 (2021) 71–73. doi:10.1016/j.conbuildmat.2020.121544.
670 [51] M. Pavlíková, L. Zemanová, J. Pokorný, M. Záleská, O. Jankovský, M. Lojka, Z. Pavlík,
671 Influence of wood-based biomass ash admixing on the structural, mechanical, hygric, and
672 thermal properties of air lime mortars, Materials (Basel). 12 (2019).
673 doi:10.3390/ma12142227.
674 [52] Z. Cheng, Y. Wang, J. Zhao, C. Huang, Gas Permeability Prediction of Mortar Samples

675 Based on Different Methods, Crystals. 12 (2022) 1–15. doi:10.3390/cryst12050581.
676 [53] Y. Wu, G. Gong, C.W. Yu, Z. Huang, Proposing ultimate moisture buffering value (UMBV)
677 for characterization of composite porous mortars, Constr. Build. Mater. 82 (2015) 81–88.
678 doi:10.1016/j.conbuildmat.2015.02.058.
679 [54] E. Latif, M. Lawrence, A. Shea, P. Walker, Moisture buffer potential of experimental wall
680 assemblies incorporating formulated hemp-lime, Build. Environ. 93 (2015) 199–209.
681 doi:10.1016/j.buildenv.2015.07.011.
682 [55] C. Shi, H. Zhang, Y. Xuan, Experimental investigation of thermal properties and moisture
683 buffering performance of composite interior finishing materials under different airflow
684 conditions, Build. Environ. 160 (2019). doi:10.1016/j.buildenv.2019.106175.
685 [56] T. Santos, L. Nunes, P. Faria, Production of eco-efficient earth-based plasters: Influence of
686 composition on physical performance and bio-susceptibility, J. Clean. Prod. 167 (2017) 55–
687 67. doi:10.1016/j.jclepro.2017.08.131.
688 [57] R. Zhang, X. Cheng, P. Hou, Z. Ye, Influences of nano-TiO2 on the properties of cement-
689 based materials: Hydration and drying shrinkage, Constr. Build. Mater. 81 (2015) 35–41.
690 doi:10.1016/j.conbuildmat.2015.02.003.
691 [58] S. Banerjee, D.D. Dionysiou, S.C. Pillai, Self-cleaning applications of TiO2 by photo-
692 induced hydrophilicity and photocatalysis, Appl. Catal. B Environ. 176–177 (2015) 396–428.
693 doi:10.1016/j.apcatb.2015.03.058.
694 [59] M. Dell'Edera, C. Lo Porto, I. De Pasquale, F. Petronella, M.L. Curri, A. Agostiano, R.
695 Comparelli, Photocatalytic TiO2-based coatings for environmental applications, Catal.
696 Today. 380 (2021) 62–83. doi:10.1016/j.cattod.2021.04.023.
697 [60] H.L. Huang, C.C. Lin, K. Hsu, Comparison of resistance improvement to fungal growth on
698 green and conventional building materials by nano-metal impregnation, Build. Environ. 93
699 (2015) 119–127. doi:10.1016/j.buildenv.2015.06.016.
700 [61] G.B. Goffredo, B. Citterio, F. Biavasco, F. Stazi, S. Barcelli, P. Munafò, Nanotechnology on
701 wood : The effect of photocatalytic nanocoatings against Aspergillus niger, J. Cult. Herit. 27
702 (2017) 125–136. doi:10.1016/j.culher.2017.04.006.
703 [62] M.Z. Guo, T.C. Ling, C.S. Poon, Nano-TiO2-based architectural mortar for NO removal and
704 bacteria inactivation: Influence of coating and weathering conditions, Cem. Concr. Compos.
705 36 (2013) 101–108. doi:10.1016/j.cemconcomp.2012.08.006.
706 [63] E. Gablech, Z. Fohlerová, K. Švec, F. Zaleš, O. Benada, O. Kofroňová, J. Pekárková, O.
707 Caha, I. Gablech, J. Gabriel, J. Drbohlavová, Selenium nanoparticles with boron salt-based
708 compound act synergistically against the brown-rot Serpula lacrymans, Int. Biodeterior.

Biodegrad. 169 (2022). doi:10.1016/j.ibiod.2022.105377.
[64] A. Gandolfo, V. Bartolomei, E. Gomez Alvarez, S. Tlili, S. Gligorovski, J. Kleffmann, H. Wortham, The effectiveness of indoor photocatalytic paints on NOx and HONO levels, Appl. Catal. B Environ. 166–167 (2015) 84–90. doi:10.1016/j.apcatb.2014.11.011.
[65] R. Zouzelka, J. Rathousky, Photocatalytic abatement of NOx pollutants in the air using commercial functional coating with porous morphology, Appl. Catal. B Environ. 217 (2017) 466–476. doi:10.1016/j.apcatb.2017.06.009.
[66] M. Pierpaoli, M.L. Ruello, Indoor Air Quality: A Bibliometric Study, Sustainability. 10 (2018) 3830. doi:https://doi.org/10.3390/su10113830.
[67] M. Pierpaoli, X. Zheng, V. Bondarenko, G. Fava, M.L. Ruello, Paving the Path to A Sustainable and Efficient SiO 2 / TiO 2 Photocatalytic Composite, Environments. (2019) 1–14.
[68] H. Wang, K. Li, J. Li, Y. Sun, F. Dong, Photochemical Transformation Pathways of Nitrates from Photocatalytic NOx Oxidation: Implications for Controlling Secondary Pollutants, Environ. Sci. Technol. Lett. (2021) 873–877. doi:10.1021/acs.estlett.1c00661.
[69] J.F. González-Sánchez, B. Taşcı, J.M. Fernández, Navarro-Blasco, J.I. Alvarez, Improvement of the depolluting and self-cleaning abilities of air lime mortars with dispersing admixtures, J. Clean. Prod. 292 (2021). doi:10.1016/j.jclepro.2021.126069.
[70] A.M. Kaja, H.J.H. Brouwers, Q.L. Yu, NOx degradation by photocatalytic mortars: The underlying role of the CH and C-S-H carbonation, Cem. Concr. Res. 125 (2019). doi:10.1016/j.cemconres.2019.105805.
[71] E. Jimenez-Relinque, J.R. Rodriguez-Garcia, A. Castillo, M. Castellote, Characteristics and efficiency of photocatalytic cementitious materials: Type of binder, roughness and microstructure, Cem. Concr. Res. 71 (2015) 124–131. doi:10.1016/j.cemconres.2015.02.003.
[72] C. Giosuè, M. Pierpaoli, A. Mobili, M.L. Ruello, F. Tittarelli, Multifunctional Lightweight Mortars for Indoor Applications to Improve Comfort and Health of Occupants: Thermal Properties and Photocatalytic Efficiency, Front. Mater. 7 (2020) 1–10. doi:10.3389/fmats.2020.00255.
[73] Y. Xiao, J. Azaiez, J.M. Hill, Erroneous Application of Pseudo-Second-Order Adsorption Kinetics Model: Ignored Assumptions and Spurious Correlations, Ind. Eng. Chem. Res. 57 (2018) 2705–2709. doi:10.1021/acs.iecr.7b04724.
[74] S. Care, F. Derkx, Determination of relevant parameters influencing gas permeability of mortars, Constr. Build. Mater. 25 (2011) 1248–1256. doi:10.1016/j.conbuildmat.2010.09.028.